

Bimodal quantitative relationships between histone modifications for X-linked and autosomal loci

Ruslan I. Sadreyev^{a,b}, Eda Yildirim^{a,c,d}, Stefan F. Pinter^{a,c,d}, and Jeannie T. Lee^{a,b,c,d,1}

^aDepartment of Molecular Biology, Massachusetts General Hospital, Boston, MA 02114; Departments of ^bPathology and ^dGenetics, Harvard Medical School, Boston, MA 02114; and ^cHoward Hughes Medical Institute, Boston, MA 02114

Edited by Mark Groudine, Fred Hutchinson Cancer Research Center, Seattle, WA, and approved February 22, 2013 (received for review September 20, 2012)

Gene expression is controlled by coordinated action of many epigenetic mechanisms including covalent histone modifications. Although numerous recurrent patterns of colocalized histone modifications have been associated with specific gene expression states, interrelationships between individual modifications are largely unknown. Here, we analyze quantitative relationships between colocalized histone marks during embryonic stem cell (ESC) differentiation and find that, for autosomal genes, these densities follow bimodal patterns. Analysis of repressive H3K27me3 and activating H3K4me3 modifications reveals the expected anticorrelation between them at active promoters but an unexpected positive correlation at inactive promoters. The two trends connect in a region corresponding to bivalent genes. Interestingly, this region is characterized by maximal H3K27 methylation. Resolving gene bivalency during ESC differentiation does not conform to the expected model of two marks as counteracting and competing forces. Although activated genes acquire H3K4me3 and lose H3K27me3, repressed genes lose H3K4me3 without gaining H3K27me3. The behavior of X-linked genes also deviates from expected models. Allele-specific analysis of chromatin modifications during X-chromosome inactivation (XCI) suggests that the silencing machinery focuses on active genes and depletion of H3K4me3 and that H3K27me3 is most significant during establishment of gene silencing. Our analysis reveals nontrivial relationships between H3K4me3 and H3K27me3, reveals unique aspects of gene bivalency, and demonstrates that XCI does not conform neatly to autosomal models.

embryonic stem cells | allele-specific ChIP-seq

Epigenetic regulation is implemented by collaboration among many factors, including transcription factors and chromatin complexes that enzymatically modify histone tails (1–3). Histone tail modifications have been correlated with different steps of transcription, including H3K4me3 with initiation, H3K36me3 with elongation, and H4 lysine acetylation with hypertranscription (4). H3K9me3 and H3K27me3 have, by contrast, been associated with repression in constitutive and facultative heterochromatin, respectively. The ability to correlate single histone modifications with expression states has led to the debated concept of a “histone code” (4, 5): the idea that combinations of two or more modifications would result in specific functional readouts. One popular example has been the “bivalent domain,” a chromatin domain often at the 5′ ends of genes within CpG islands that are marked paradoxically by both activating H3K4me3 and repressive H3K27me3 (6, 7). Bivalent domains define developmentally critical genes in gametes, embryonic stem cells (ESCs), and the early embryo. By carrying two marks, bivalent domains keep lineage-specific genes repressed yet poised for activation or repression during differentiation. Genomewide analysis has also produced finer-grain correlations between chromatin and gene expression, revealing numerous recurring combinations of colocalized chromatin marks (8).

Their presence suggests interrelationships between different chromatin modifications. In a few instances, specific protein regulators of cross-talk between histone modifications have been identified (3, 9). Recent work, based largely on linear modeling, led to the concept of quantitative transcriptional regulation via chromatin modifications and transcription factors, where their

levels define precise transcription output in a continuous fashion (10–15). However, combinations of multiple histone marks might produce nontrivial transcriptional readouts if levels of chromatin marks show nonlinear and nonunique dependencies on each other.

Hints of such dependencies may, for example, be gleaned from recent allele-specific analysis of the X-chromosome (14, 16). Unlike autosomes, the mammalian X is subject to two types of “dosage compensation” due to dosage differences between the sexes. First, to compensate for X-linked differences between females and males, female cells undergo X-chromosome inactivation (XCI) (17), a process that depends on Xist RNA (18), and recruitment of Polycomb repressive complex 2 (PRC2) (19–22), the epigenetic complex that trimethylates H3K27 (2). Establishment of XCI is marked by spreading of H3K27me3 along the inactive X (Xi) (19–22). However, although H3K27me3 levels increase during establishment of XCI, maintenance does not depend on high concentrations (16). Thus, H3K27me3 densities do not track quantitatively with gene repression. The halving of total X-expression during XCI necessitates a second dosage compensation to balance X and autosomal dosages. This second process involves hyperactivation of the active X (Xa) (23, 24) and involves increased H3K4me3, H3K36me3, and POL-II (RNA polymerase II), but the increases do not scale linearly with transcription (14). Given these findings, herein we address quantitative relationships between chromatin marks on a genomewide scale, focusing on levels of H3K4me3 and H3K27me3 as continuous variables and assessing differences between the X-chromosome and autosomes.

Results and Discussion

Quantitative Relationships for Autosomal Genes. First, we examined the association of histone modification and POL-II occupancies with autosomal transcription output. We used allele-specific ChIP-seq data from female mouse embryonic fibroblasts (MEFs) from an F₁ cross between *Mus musculus* (mus) and *Mus castaneus* (cas) (14, 16). We also used data from hybrid female ESCs on day 0 (d0) and day 7 (d7) of cell differentiation. We analyzed densities of H3K27me3, H3K4me3, phospho-serine-5 POL-II [POL-II-S5P; associated with poised POL-II at transcription start sites (TSSs)], H3K36me3 (associated with transcription elongation), and phospho-serine-2 POL-II (POL-II-S2P; associated with elongation). Transcription output was inferred from RNA-seq data in d0 female mouse ESCs and female fibroblasts (25) using TopHat and Cufflinks methods (26, 27), and was expressed as fragments per kilobase per million (FPKM) for RefSeq mouse genes.

As expected, in general, gene expression levels had a positive quantitative relationship with H3K4me3, H3K36me3, and POL-II levels but a negative relationship with H3K27me3 levels. The dependencies of autosomal gene expression on mark densities in d0 ESCs (Fig. 1A–D) and MEFs (Fig. 1E–H) were linearized on a log-log scale, consistent with previous analyses (11, 14). Notably, H3K27me3 (Fig. 1C) had less pronounced correlation with

Author contributions: S.F.P. and J.T.L. designed research; R.I.S., E.Y., and S.F.P. performed research; R.I.S. and J.T.L. analyzed data; and R.I.S. and J.T.L. wrote the paper.

The authors declare no conflict of interest.

This article is a PNAS Direct Submission.

¹To whom correspondence should be addressed. E-mail: lee@molbio.mgh.harvard.edu.

This article contains supporting information online at www.pnas.org/lookup/suppl/doi:10.1073/pnas.1216449110/-DCSupplemental.

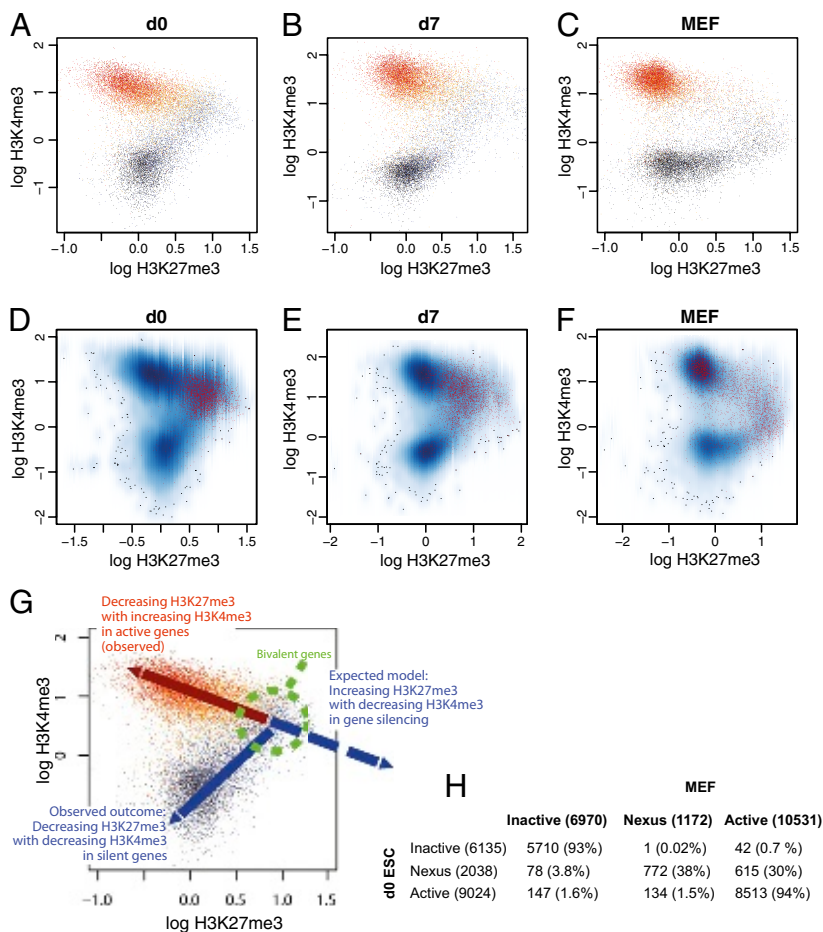


Fig. 3. Quantitative relationships between H3K4me3 and H3K27me3. (A–C) Densities of H3K4me3 and H3K27me3 around autosomal TSSs are shown as scatterplots in ESCs and MEF. Point colors indicate the level of gene expression in \log_{10} scale. Cold colors (black to light blue), inactive genes (FPKM < 1.0); warm colors (yellow to brown), active genes (FPKM > 1.0). (D–F) Positioning of bivalent genes (red points) in indicated cells. Point densities in each scatterplot are indicated by shades of blue. (G) Expected vs. observed models of quantitative relationships between H3K4me3 and H3K27me3. Observed relationships between the two marks are shown as solid red and blue arrows for active and inactive genes, respectively. The expected model would consist of a single continuous line formed by the solid red arrow and dashed blue arrow. Bivalent promoters (green circle) located within nexus. (H) Migration of genes between branches during differentiation. Three nonoverlapping approximate areas of the H3K4me3 vs. H3K27me3 plot were conservatively selected as active branch (H3K4me3 and H3K27me3 densities $>10^{0.5} \sim 3.16$ and $<10^{0.5}$, respectively), inactive branch (densities <1.0 and $<10^{0.5}$, respectively), and nexus (H3K4me3 density >1.0 , H3K27me3 density $>10^{0.75}$). Each row corresponds to the numbers (percentages) of promoters on d0 that migrate to a new region in MEF. Parentheses indicate total number of genes on d0 and in MEF. Fractions do not sum up to 100% because the conservatively defined areas do not fully cover the scatterplot.

That is, in the upper branch harboring active genes, there was an expected anticorrelation between the two marks: an increase of H3K4me3 generally paralleled a decrease of H3K27me3 (upper left direction in the plot), and this trend was predictive of a general increase in gene expression (redder colors). However, in the lower branch harboring inactive genes, there was an unexpected positive correlation between the two opposing marks: a depletion of H3K4me3 was also accompanied by depletion, rather than gain, of H3K27me3. The most silent genes (blackest points) were generally more depleted for H3K27me3 than less silent genes (light blue points). The exact epigenetic mechanisms of these two modes of coordination between H3K4me3 and H3K27me3, through direct interaction of enzymatic machineries or otherwise, will be of future interest.

A prominent feature of all plots was a “nexus” between active and inactive branches (Fig. 3 A–G). This nexus occurred in the region of high H3K27me3 (density of ~ 10) and relatively marginal H3K4me3 (density of ~ 1 –3). Importantly, the nexus was the only point of connection between the branches and was what gave the plots a distinct rotated V-shape; there was no connection

at lower H3K27me3. This structure suggested that H3K4me3 is the main driving factor in H3K4me3/H3K27me3 dynamics: H3K4me3 levels uniquely determined the branch, even at the promoters with a considerable H3K27me3 density of up to ~ 3 (Fig. 3 A–G). Gene activity was predicted by high H3K4me3 and silencing by low H3K4me3. Correspondingly, H3K4me3 was the stronger driving factor for the level of gene expression, consistent with modeling results (Fig. 1I). On the other hand, there was no unique correspondence between H3K27me3 level and gene expression status: the same H3K27me3 density can be observed in both active and inactive branches.

The nexus region between active and inactive branches may be functionally important. Indeed, on d0, this region was populated largely by bivalent genes (Fig. 3D, red data points), which have the potential of becoming either active or inactive during differentiation (6). Consistent with previous characterizations (6), the nexus was strongly enriched with both general and specialized developmental factors, including homeobox genes [false discovery rate (FDR) of 5.3×10^{-114} by the DAVID functional annotation tool (33)], Forkhead (FDR = 2.7×10^{-6}), and transcription

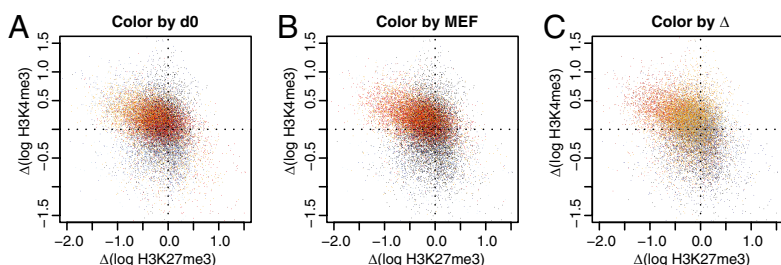
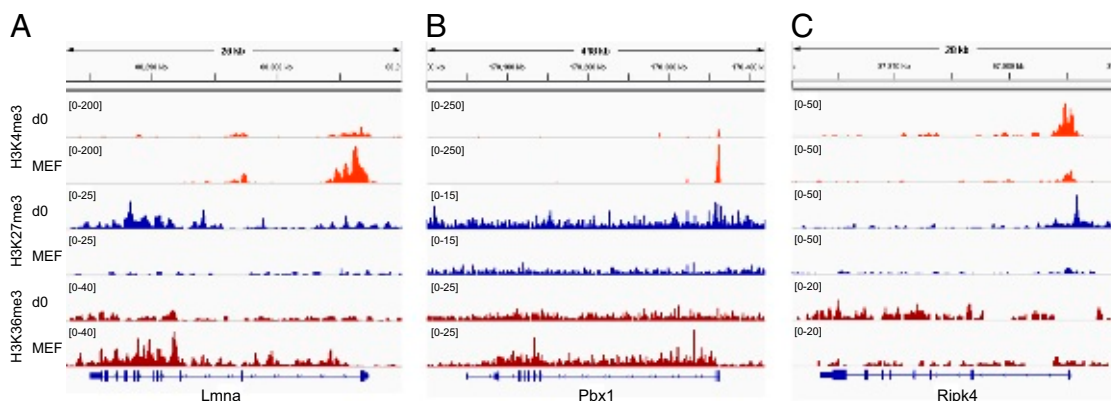


Fig. 4. Coordinated changes of H3K4me3 and H3K27me3 during differentiation. Changes around autosomal TSSs between d0 ESC and MEF are shown in the scatterplots, with points colored according to expression in \log_{10} scale (cold colors, negative; warm colors, positive). $\Delta(\log \text{H3K27me3})$, $\Delta(\log \text{H3K4me3})$ denote the \log_{10} difference (d0 subtracted from MEF). Color by expression in d0 ESC (A) and MEF (B). (C) Color by the change of expression $\Delta(\log \text{FPKM})$ during differentiation. Numbers and fractions of genes in quadrants showing different directions of mark changes: upper left, 9,922 (49%); lower left, 4,393 (22%); upper right, 2,877 (14%); lower right, 3,234 (16%).



bivalency, however, many genes stayed within the nexus after differentiation into MEFs, a clonal population that is presumptively more homogeneous. In most genes assayed by Hong et al. (35), K4/K27 ratios were in the range of 0.2–5.0. In our analysis of colocalized marks, equal densities of K4me3 and K27me3 corresponded to the diagonal $x = y$ (Fig. S1A, thick green line), whereas larger or smaller K4/K27 ratios corresponded to lines parallel to the diagonal. Fig. S1A shows these lines for the ratios of 0.2 and 5.0 (thin green lines). Such lines generally cannot define a unique branch or area of the plot: points along a line can belong to multiple areas, e.g., nexus or any portion of inactive branch, suggesting that the K4/K27 ratio alone at a given promoter may not be a fully adequate criterion of gene bivalency.

Developmental Progression of Autosomal Associations Between H3K4me3 and H3K27me3. Developmental profiles revealed several trends during ESC differentiation (Fig. 3A–C). First, there was a genomewide process of polarization of chromatin states, from more versatile and diffuse patterns in ESCs to a more concentrated distribution within two regions in MEFs. This polarization involved the movement away from the nexus toward extremes of two branches: (i) region with very high H3K4me3 (densities of 10–100) and low H3K27me3 (0.1–1) (red dots, active genes); and (ii) region with low H3K4me3 (0.1–1) and low to high H3K27me3 (0.1–3) (black dots, inactive genes).

Second, as a part of this general polarization process, the nexus occupied by bivalent genes became less populated (Fig. 3A; bivalency defined by \log_{10} H3K4me3 density > 0.0 and \log_{10} H3K27me3 density > 0.75). Tracking the fate of bivalent genes within the rotated V revealed that bivalency was resolved by migration of genes toward one of two branches (Fig. 3D–F, red dots = bivalent genes), roughly correlating with the previously described resolution of gene bivalency during cell differentiation (6). The total census of genes in the nexus was comparable on d0 and d7 (9.8% and 10.9%, respectively) but decreased to 5.6% in MEFs (Fig. 3H). This movement of bivalent genes from the nexus area of maximal H3K27me3 levels into the branches implied that, unexpectedly, resolving gene bivalency during differentiation does not proceed in two opposite directions and does not involve additional methylation of H3K27. In fact, H3K27me3 levels reached a maximum at bivalent promoters.

Developmental progression of a given promoter as a point on the plane followed a few major patterns (Fig. 4C; Fig. S1B). For a large fraction of genes (residing in the area of ± 0.3 in the \log_{10} scale), the densities of H3K27me3 and H3K4me3 did not change by more than twofold (Fig. 4). However, more pronounced changes did occur in other genes. The most prominent showed an increase of H3K4me3 accompanying a decrease of H3K27me3 (Fig. 4, upper left quadrant), corresponding to the increase of gene expression through the movement along the active (upper) branch (Fig. 3A–C). These promoters could be either active or inactive on d0 (Fig. 4A) but became active in MEFs (Fig. 4B). Genes that were inactive on d0 went through a larger change in H3K4me3 density [$\Delta(\log_{10} \text{H3K4me3})$] (Fig. 4C; Fig. S1B).

Interestingly, bivalent genes that resolved into the upper branch were functionally different from active genes that migrated further upward along the upper branch during differentiation (Dataset S2 vs. Dataset S3). Among 1,201 genes of the active branch that showed greater than a twofold change in H3K4me3 and H3K27me3 densities during differentiation, the highest enrichment was observed in mitochondrial (DAVID FDR = 1.9×10^{-6}), lysosomal (FDR = 8.1×10^{-3}), and Golgi (FDR = 9.4×10^{-3}) proteins. By contrast, the 615 bivalent genes that moved into the active branch during differentiation were strongly enriched for cell adhesion molecules (FDR = 3.8×10^{-4}), genes for cell migration (FDR = 8.2×10^{-7}), and transcription factors (FDR = 1.1×10^{-13}). Additionally, 772 bivalent genes did not move out of the nexus after differentiation (Dataset S4) and were enriched in transcription factors (DAVID FDR = 4.2×10^{-29}), more than half of which were homeobox genes (FDR = 3.1×10^{-50}). The opposite movement—descent along the upper branch—was rarer (Fig. 4). Only 25 genes went

through a negative change of expression (Fig. 4C) from active state on d0 (Fig. 4A) to a less active state in MEFs (Fig. 4B); 134 genes moved from the active branch into the nexus. There was no strong enrichment in any functional category.

A second prominent change involved genes that showed a decrease of both H3K4me3 and H3K27me3 (Fig. 4; Fig. S1B; lower left quadrant). These genes were mostly inactive already in d0 ESCs and showed no change in expression during differentiation. This pattern corresponded to movement along the inactive branch in Fig. 3. This category applied to 234 genes that already resided in the lower branch on d0 and showed greater than twofold change in H3K27me3 density, resulting in a descent along lower branch (Dataset S5). These genes often had highly cell type-specific expression, such as specialized signal peptides and their receptors (DAVID FDR = 3.4×10^{-3}). In addition, 78 genes moved from the nexus into the lower branch (Dataset S6). These genes were enriched for transmembrane proteins (FDR = 1.1×10^{-4}) such as the cadherin genes (FDR = 1.1×10^{-13}) known to be involved in cell–cell recognition of neurons.

Another type of change involved genes showing a decrease in H3K4me3 with no change or a moderate increase of H3K27me3. These genes showed low or no expression at d0 (Fig. 4A) and became silent in MEFs (Fig. 4B), with mostly negative changes in expression (Fig. 4C; Fig. S1B). This category mainly corresponded to downward movement within the nexus or switching from upper to lower branches. Switching between branches during differentiation was a relatively rare event: only ~1% of genes switched branches during differentiation (Datasets S7 and S8; Fig. 3H). With only one intermediate time point (d7), it could not be determined whether gene activation or repression must generally proceed through the nexus. Only one of these genes (*Slc6a7*) was found in the nexus on d7, whereas the majority of these genes was still in the same branch (30 of 42 genes switched from inactive to active and 107 of 142 genes switched from active to inactive branch).

Fig. 5 shows specific examples of epigenetic progression during differentiation. Lamin A (*Lmna*; Fig. 5A) was active on d0 and moved along active branch toward greater activity during differentiation. The homeobox gene, *Pbx1* (Fig. 5B), was bivalent on d0 and migrated out of the nexus into the active branch during differentiation (became activated). The kinase gene, *Ripk4* (Fig. 5C), was bivalent on d0 and migrated into the inactive branch (became silenced).

Divergent Modes of Regulation on Active and Inactive X-Chromosomes. The relatively poor correlation of gene silencing with H3K27me3 may be surprising, given that the establishment of silencing on the Xi involves PRC2 and spread of H3K27me3 (16, 19–22). An interesting aspect of dosage compensation is that, although H3K27me3 occupancies are hugely increased during establishment of Xi, maintenance of Xi does not depend on a high concentration of H3K27me3. We therefore asked if the modes of regulation differed for X-linked genes, with respect to both Xa and Xi.

To separately survey Xa and Xi, we analyzed allele-specific ChIP-seq data (14, 16) for relationships between histone modifications (Fig. 6). In the cell lines used, Xa is of paternal and Xi of maternal origin (14, 16). We examined promoters on a representative autosome, chr13 (Fig. 6A–C), Xa (paternal, Fig. 6D–F), and Xi (maternal, Fig. 6G–I). Although paternal and maternal allelic mark densities on autosomes behaved similarly to each other and to composite mark densities (Fig. 3), the progression of epigenetic events on the two X chromosomes was different. Patterns on Xa (Fig. 6D–F) resembled chr13 (Fig. 6A–C), with upper and lower branches meeting in the area of high H3K27me3 and marginal H3K4me3. On Xa, the nexus also corresponded to bivalent genes on d0 (Fig. 6D), many of which migrated to one of two branches on d7 (Fig. 6E) and in MEFs (Fig. 6F), as was the case for autosomal genes (Fig. 3).

The Xi behaved differently. As expected, the future Xi looked similar to Xa and autosomes on d0 (pre-XCI state; Fig. 6G). However, on d7, Xi promoters that were active on d0 showed higher levels of H3K27me3, consistent with the recruitment of PRC2 (Fig. 6H, yellow points). Levels of H3K4me3 were not strongly affected by this H3K27 methylation and stayed largely

similar to those on d0 (Fig. 6*H*, yellow points), a notable deviation from the general anticorrelation of H3K4me3 and H3K27me3 observed elsewhere in the genome. On the other hand, promoters of silent genes in the lower branch on d0 did not show elevation of H3K27me3 during differentiation (Fig. 6*H*, light blue points). This absence of additional H3K27 methylation suggested that PRC2 during XCI selectively targets genes that are active on d0. Bivalent genes on Xi—unlike their autosomal and Xa counterparts—did not show a substantial change of mark densities on d7.

Furthermore, in MEFs, the Xi promoters showed a compact grouping in the area of marginal H3K27me3 occupancy (levels around 1.0) and strongly depleted H3K4me3 (Fig. 6*J*). No Xi promoters had an H3K4me3 density higher than 1.0, except for 10 promoters that escaped XCI (16, 25, 36). This area corresponded to the branches on Xa and autosomes bearing silent genes, as might be expected. However, the relatively low H3K27me3 levels were surprising, given that the Xi has been shown to be enriched cytologically for PRC2 and H3K27me3. This pattern in MEFs suggested that strong demethylation of H3K4me3 plays an important role in XCI, and after differentiation, H3K4 demethylation may mediate the maintenance of silent gene state on Xi more directly than H3K27 methylation, whose levels were often low to marginal.

Together, these findings lead to several conclusions. First, Xa and associated genic hypertranscription follow quantitative relationships akin to those for active genes on autosomes. Second, the relationship on Xi with the process of XCI is more complex and does not follow simple quantitative relationships seen for general autosomal loci. On Xi, there is first an intensive H3K27 methylation uncoupled from the level of H3K4me3, which remains surprisingly high and largely unaffected during the establishment phase (d0–d7). The massive H3K27 methylation is consistent with the idea that this histone modification is most significant during cell differentiation and the initial establishment of gene silencing. Subsequently, during the maintenance stage (i.e., in MEFs), there is depletion of H3K4me3 to the levels of silent genes on autosomes (per autosomal inactive mode). During this

stage, H3K27me3 occupancy is reduced and maintained at largely marginal levels, which may suggest that maintenance of H3K4me3 depletion plays a larger role at this stage. Because changes on Xi were observed only for genes that were previously active on d0 and no further changes occurred on genes that were inactive on d0, we suggest that the XCI machinery is selectively targeted to active genes on the future Xi. In summary, we identified bimodal quantitative relationships between histone marks that apply to genes on autosomes and Xa but are modified for those on Xi. Inclusion of other epigenetic marks in further analyses should yield more insights into relationships between chromatin modifications, as well as the corresponding epigenetic machinery.

Methods

ChIP-seq data have been described (GEO accession no. GSE36905). Read alignment and allele-specific coverage calculation were performed as previously described (14, 16). RNA-seq reads by Yang et al. (25) (NCBI SRA accession no. SRA010053) were aligned to mm9 genome using TopHat (26) with default parameters, except for using arguments: no-novel-juncs and min-isoform-fraction 0. The resulting alignments were used to calculate FPKM values using Cufflinks (27) with default parameters, except for setting: min-isoform-fraction 0. As a cutoff for active expression, we chose an FPKM of 1.0 corresponding to the boundary between two regimes of FPKM correlation to composite POL-II density on a gene: the absence of dependency at low values, consistent with readout fluctuations for silent genes, and positive correlation at higher values, consistent with active transcription (14). Choosing an FPKM cutoff of 0 produced similar results. Linear models were built for the \log_{10} of gene FPKM based on the \log_{10} of corresponding occupancy densities of histone modifications and POL-II.

ACKNOWLEDGMENTS. We thank the J.T.L. laboratory and Brad Bernstein for valuable discussion. This work was supported by the Massachusetts General Hospital Executive Committee on Research Medical Discovery Fund (E.Y.), Deutsche Forschungsgemeinschaft (S.F.P.), and National Institutes of Health Grant RO1-GM090278 (to J.T.L.). J.T.L. is an investigator of the Howard Hughes Medical Institute.

- Zhou VW, Goren A, Bernstein BE (2011) Charting histone modifications and the functional organization of mammalian genomes. *Nat Rev Genet* 12(1):7–18.
- Bonasio R, Tu S, Reinberg D (2010) Molecular signals of epigenetic states. *Science* 330(6004):612–616.
- Suganuma T, Workman JL (2008) Crosstalk among histone modifications. *Cell* 135(4):604–607.
- Rando OJ (2012) Combinatorial complexity in chromatin structure and function: Revisiting the histone code. *Curr Opin Genet Dev* 22(2):148–155.
- Strahl BD, Allis CD (2000) The language of covalent histone modifications. *Nature* 403(6765):41–45.
- Bernstein BE, et al. (2006) A bivalent chromatin structure marks key developmental genes in embryonic stem cells. *Cell* 125(2):315–326.
- Vastenhouw NL, Schier AF (2012) Bivalent histone modifications in early embryogenesis. *Curr Opin Cell Biol* 24(3):374–386.
- Ernst J, Kellis M (2010) Discovery and characterization of chromatin states for systematic annotation of the human genome. *Nat Biotechnol* 28(8):817–825.
- Lee JS, et al. (2007) Histone crosstalk between H2B monoubiquitination and H3 methylation mediated by COMPASS. *Cell* 131(6):1084–1096.
- Ouyang Z, Zhou Q, Wong WH (2009) ChIP-Seq of transcription factors predicts absolute and differential gene expression in embryonic stem cells. *Proc Natl Acad Sci USA* 106(51):21521–21526.
- Karlič R, Chung HR, Lasserre J, Vlahovicek K, Vingron M (2010) Histone modification levels are predictive for gene expression. *Proc Natl Acad Sci USA* 107(7):2926–2931.
- Cheng C, Gerstein M (2012) Modeling the relative relationship of transcription factor binding and histone modifications to gene expression levels in mouse embryonic stem cells. *Nucleic Acids Res* 40(2):553–568.
- Tippmann SC, et al. (2012) Chromatin measurements reveal contributions of synthesis and decay to steady-state mRNA levels. *Mol Syst Biol* 8:593.
- Yildirim E, Sadreyev RI, Pinter SF, Lee JT (2012) X-chromosome hyperactivation in mammals via nonlinear relationships between chromatin states and transcription. *Nat Struct Mol Biol* 19(1):56–61.
- Mikkelsen TS, et al. (2007) Genome-wide maps of chromatin state in pluripotent and lineage-committed cells. *Nature* 448(7153):553–560.
- Pinter SF, et al. (2012) Spreading of X chromosome inactivation via a hierarchy of defined Polycomb stations. *Genome Res* 22(10):1864–1876.
- Lyon MF (1971) Possible mechanisms of X chromosome inactivation. *Nat New Biol* 232(34):229–232.
- Brown CJ, et al. (1992) The human XIST gene: Analysis of a 17 kb inactive X-specific RNA that contains conserved repeats and is highly localized within the nucleus. *Cell* 71(3):527–542.
- Mak W, et al. (2002) Mitotically stable association of polycomb group proteins eed and enx1 with the inactive x chromosome in trophoblast stem cells. *Curr Biol* 12(12):1016–1020.
- Wang J, et al. (2001) Imprinted X inactivation maintained by a mouse Polycomb group gene. *Nat Genet* 28(4):371–375.
- Plath K, et al. (2003) Role of histone H3 lysine 27 methylation in X inactivation. *Science* 300(5616):131–135.
- Zhao J, Sun BK, Erwin JA, Song JJ, Lee JT (2008) Polycomb proteins targeted by a short repeat RNA to the mouse X chromosome. *Science* 322(5902):750–756.
- Nguyen DK, Distche CM (2006) Dosage compensation of the active X chromosome in mammals. *Nat Genet* 38(1):47–53.
- Lin H, et al. (2007) Dosage compensation in the mouse balances up-regulation and silencing of X-linked genes. *PLoS Biol* 5(12):e326.
- Yang F, Babak T, Shendure J, Distche CM (2010) Global survey of escape from X inactivation by RNA-sequencing in mouse. *Genome Res* 20(5):614–622.
- Trapnell C, Pachter L, Salzberg SL (2009) TopHat: Discovering splice junctions with RNA-Seq. *Bioinformatics* 25(9):1105–1111.
- Trapnell C, et al. (2010) Transcript assembly and quantification by RNA-Seq reveals unannotated transcripts and isoform switching during cell differentiation. *Nat Biotechnol* 28(5):511–515.
- Boyer LA, Mathur D, Jaenisch R (2006) Molecular control of pluripotency. *Curr Opin Genet Dev* 16(5):455–462.
- Pan G, et al. (2007) Whole-genome analysis of histone H3 lysine 4 and lysine 27 methylation in human embryonic stem cells. *Cell Stem Cell* 1(3):299–312.
- Pietersen AM, van Lohuizen M (2008) Stem cell regulation by polycomb repressors: Postponing commitment. *Curr Opin Cell Biol* 20(2):201–207.
- Surface LE, Thornton SR, Boyer LA (2010) Polycomb group proteins set the stage for early lineage commitment. *Cell Stem Cell* 7(3):288–298.
- Zhao XD, et al. (2007) Whole-genome mapping of histone H3 Lys4 and 27 trimethylations reveals distinct genomic compartments in human embryonic stem cells. *Cell Stem Cell* 1(3):286–298.
- Huang W, Sherman BT, Lempicki RA (2009) Systematic and integrative analysis of large gene lists using DAVID bioinformatics resources. *Nat Protoc* 4(1):44–57.
- Mendenhall EM, et al. (2010) GC-rich sequence elements recruit PRC2 in mammalian ES cells. *PLoS Genet* 6(12):e1001244.
- Hong SH, et al. (2011) Cell fate potential of human pluripotent stem cells is encoded by histone modifications. *Cell Stem Cell* 9(1):24–36.
- Carrel L, Willard HF (2005) X-inactivation profile reveals extensive variability in X-linked gene expression in females. *Nature* 434(7031):400–404.